

Organics Exposure in Orbit (OREOcube): A Next-Generation Space Exposure Platform

Andreas Elsaesser,^{*,†} Richard C. Quinn,^{*,‡} Pascale Ehrenfreund,[†] Andrew L. Mattioda,[§] Antonio J. Ricco,^{*,§} Jason Alonzo,^{‡,||} Alex Breitenbach,^{‡,⊥} Yee Kim Chan,^{‡,⊥} Aurelien Fresneau,[†] Farid Salama,[§] and Orlando Santos[§]

[†]Leiden Institute of Chemistry, Leiden University, Leiden 2333CC, The Netherlands

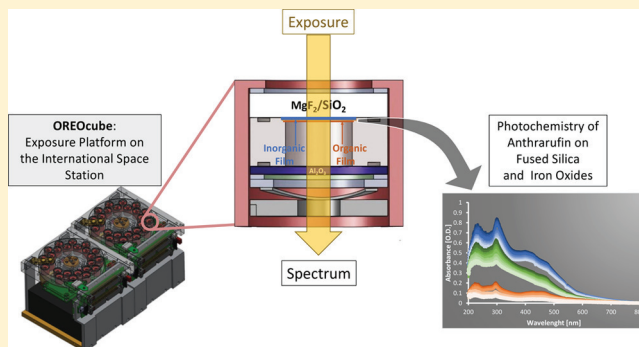
[‡]Carl Sagan Center, SETI Institute, NASA Ames Research Center, Moffett Field, California 94035, United States

[§]NASA Ames Research Center, Moffett Field, California 94035, United States

^{||}Department of Physics and Astronomy, California State Polytechnic University, Pomona, California 91768, United States

[⊥]San Jose State University, San Jose, California 95112, United States

ABSTRACT: The OREOcube (ORganics Exposure in Orbit cube) experiment on the International Space Station (ISS) will investigate the effects of solar and cosmic radiation on organic thin films supported on inorganic substrates. Probing the kinetics of structural changes and photomodulated organic–inorganic interactions with real-time in situ UV–visible spectroscopy, this experiment will investigate the role played by solid mineral surfaces in the (photo)chemical evolution, transport, and distribution of organics in our solar system and beyond. In preparation for the OREOcube ISS experiment, we report here laboratory measurements of the photostability of thin films of the 9,10-anthraquinone derivative anthrarufin (51 nm thick) layered upon ultrathin films of iron oxides magnetite and hematite (4 nm thick), as well as supported directly on fused silica. During irradiation with UV and visible light simulating the photon flux and spectral distribution on the surface of Mars, anthrarufin/iron oxide bilayer thin films were exposed to CO₂ (800 Pa), the main constituent (and pressure) of the martian atmosphere. The time-dependent photodegradation of anthrarufin thin films revealed the inhibition of degradation by both types of underlying iron oxides relative to anthrarufin on bare fused silica. Interactions between the organic and inorganic thin films, apparent in spectral shifts of the anthrarufin bands, are consistent with presumed free-electron quenching of semiquinone anion radicals by the iron oxide layers, effectively protecting the organic compound from photodegradation. Combining such in situ real-time kinetic measurements of thin films in future space exposure experiments on the ISS with postflight sample return and analysis will provide time-course studies complemented by in-depth chemical analysis. This will facilitate the characterization and modeling of the chemistry of organic species associated with mineral surfaces in astrobiological contexts.



1. INTRODUCTION

1.1. Motivation: Relevance of Photochemical Processing of Organics in Outer Space. Ground- and space-based astronomical observations have identified more than 180 different types of molecules in our own as well as distant galaxies, many of them carbonaceous in nature.^{1–3} Carbonaceous materials are found in gaseous and solid form and include polycyclic aromatic hydrocarbons (PAHs), nanodiamonds, and fullerenes. Complex carbon molecules that are formed in interstellar clouds and circumstellar environments evolve and are integrated into star-system material during stellar and planetary formation processes. Some of the “leftover” material from the formation of our solar system (i.e., not integrated into planets) was carried to young planetary surfaces, including Earth’s after it cooled and solidified, by asteroids, comets, and their fragments,^{4,5} delivering substantial amounts of the

carbonaceous raw materials important for life.^{6,7} Among the organic compounds found in meteorites are purines, pyrimidines and polyols, fatty acids, and amino acids, all precursor molecules for life.^{3,8,9}

Because of the role of photochemical reactions in the formation, processing, and destruction of such carbonaceous compounds prior to their arrival on Earth, the study of the reactions, destruction, and longevity of these organics in the space environment is of fundamental interest.¹⁰ The search for biomarkers that might reveal extant or extinct life on other solar system bodies also engenders interest in the outer space

Received: March 28, 2014

Revised: May 20, 2014

Published: May 22, 2014

longevity of organic molecules characteristic of life as we know it.

While the solar spectrum can be partly reproduced in the laboratory, it is quite challenging to faithfully create the entire radiation spectrum including the appropriate levels of vacuum ultraviolet and to maintain this radiation at appropriate intensities for weeks, months, and longer in the laboratory in order to study the often-slow degradation of organics in an artificial space “environment”.^{11,12} Furthermore, it is impossible to simultaneously subject the organic materials to the complex ionizing cosmic radiation environment of outer space, which is composed of multiple particle types, each with its own unique energy spectrum and which may contribute in some cases to the overall processing of organics in the space environment.

To provide a completely accurate outer space environment for extended durations, exposure experiments in low Earth orbit have been conducted in the last decades in order to examine the consequences of actual space conditions including combinations of solar and cosmic radiation, space vacuum, and microgravity. A series of successful experiments performed on International Space Station (ISS) external platforms have provided insights into the evolution of organic and biological materials in space and planetary environments.^{13,14} ISS exposure experiments have included studies of biomarker stabilities including amino acids and nucleobases, as well as PAHs.^{11,15} Until recently, most of these studies relied on detailed characterization of the organic materials prior and subsequent to their space exposure period; kinetic information, apart from that gleaned from the reaction end points, is not available with this approach.

1.2. In-Situ Studies of Organic Photoreactions Using Real-Time Measurements. The ORganics Exposure in Orbit cube (OREOCube) is composed of a pair of identical 1U (smallest unit of a cubesat or its payload with dimensions of $10 \times 10 \times 10 \text{ cm}^3$) payload instrument packages designed for the real-time, in situ study of photochemical reactions, including kinetic data, of organic compounds and biomarkers on an ISS external platform (Figure 1). In an OREOCube experiment, optically thin film samples are measured in situ using ultraviolet (UV)–visible (vis)–near-infrared (NIR) spectroscopy (230–1000 nm) during exposure to full-spectrum solar and cosmic radiation. Samples are contained in hermetically sealed reaction cells that protect the samples from contamination until they reach outer space and can also provide relevant contacting gas environments.

OREOCube is the second generation of in situ experiments based on the space environment viability of organics (SEVO) 1U payload, which was designed for the NASA O/OREOS (Organism/ORganic Exposure to Orbital Stresses) nanosatellite.^{16,17} During the 6-month primary and 1-year extended O/OREOS mission, the photochemical processing of the PAH isoviolanthrene, the quinone anthrarufin (1,5-dihydroxyanthrarufin), and iron tetraphenylporphyrin chloride was studied in low Earth orbit; results were autonomously telemetered to Earth.^{12,18}

Expanding on the astrochemical and astrobiological studies initiated with the O/OREOS nanosatellite, the OREOCube ISS experiment is designed to investigate the roles that solid mineral surfaces play in the chemical evolution and distribution of organics in the interstellar medium, comets, meteorites, and other celestial objects. By measuring changes in the UV–vis–NIR spectra of samples as a function of time in situ, OREOCube will provide data sets that capture critical kinetic and

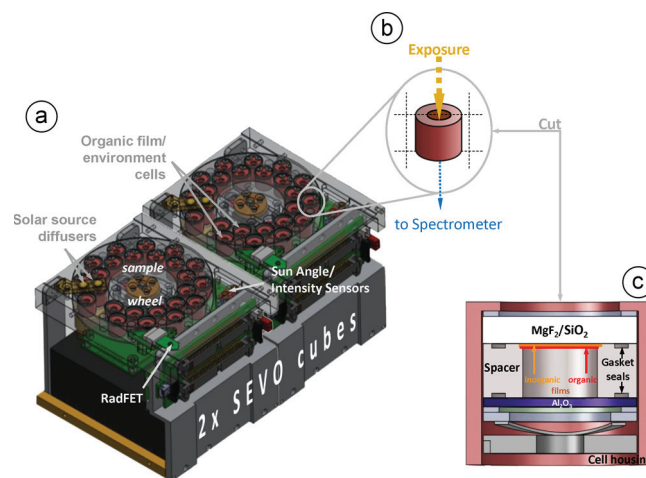


Figure 1. (a) Solid model of OREOCube organic exposure-and-monitoring system for external ISS installation. Overall dimensions: $\sim 10 \times 10 \times 20 \text{ cm}$. Each cube includes a 24-sample carousel, collection optics, motor, electronics, and UV–vis–NIR spectrometer that collects and transfers to ISS the transmission spectra of organic thin-film samples using the Sun as a light source. Samples are mounted in (b) individual sample cells with controlled internal gas-phase environments. (c) Cross-sectional view of 1 of the 24 sample cells included in each SEVO cube; sunlight enters at the top through the MgF_2 , Al_2O_3 , or SiO_2 window, and the transmitted light is collected at the bottom of the cell after passing through the lower Al_2O_3 window. The thin film under study can be supported on the underside of the Sun-facing cell window as shown, or it can be on the top side of the bottom, spectrometer-facing window (here labeled Al_2O_3) if it is preferable for the light to pass through the layers of a multilayer film in the opposite order.

mechanistic details of sample reactions that cannot be obtained with current ISS noninstrumented external exposure facilities. Combining in situ real-time kinetic measurements with postflight sample analysis will provide time-course studies as well as in-depth chemical analysis, enabling us to characterize and model the chemistry and material science of organic chemicals associated with mineral surfaces in astrobiological contexts. Here we describe the science background and considerations that drive the OREOCube investigation, the ISS payload system, and the technical details of the OREOCube samples. We present results concerning the preflight laboratory characterization of anthrarufin thin films layered upon ultrathin films of the iron oxides magnetite and hematite and fused silica.

1.3. OREOCube Science. The OREOCube experiment investigates the (photo)reactive properties of organic biomarkers as well as organic compounds of astrochemical importance (Table 1) in combination with potentially catalytic,

Table 1. OREOCube Candidate Organic Sample Classes

candidate organic materials		
porphyrins	quinones	polycyclic aromatic hydrocarbons

mineralogically relevant metal oxides (Table 2). Representative compounds from four organic sample classes (amino acids, porphyrins, polycyclic aromatic hydrocarbons (PAHs), and quinones) were investigated during the O/OREOS nanosatellite mission.¹⁶ Three of these compounds, isoviolanthrene (PAH class), iron(III)-5,10,15,20-tetraphenyl-21H,23H-porphyrin chloride (FeTPPCl; porphyrin class), and 1,5-dihydroxyanthraquinone (anthrarufin; quinone class) will be used as

Table 2. OREOCube Candidate Inorganic Samples (Catalytic Underlayers)

candidate inorganic materials	
forsterite (Mg_2SiO_4)	chromium oxide (Cr_2O_3)
fayalite (Fe_2SiO_4)	manganese oxide (MnO)
corundum (Al_2O_3)	iron and iron–nickel alloys
iron oxide(s) (Fe_xO_y)	iron sulfide (FeS_2)
titanium oxides (TiO_2)	silica (SiO_2)

OREOCube samples. OREOCube experiments will expand the science of the space-environment processing of these species by investigating their interactions in inorganic (photo)catalysis experiments.

FeTPPCL is representative of a large class of redox-active organometallic compounds, typified by porphyrins and phthalocyanines, that enable biological processes from photosynthesis to respiration. PAHs are abundant and ubiquitous in galactic and extragalactic regions, protoplanetary disks, and solar system objects, and spectral measurements indicate the presence of a large variety of individual compounds, clusters, and PAH-related molecules.^{19–21}

Members of a class of redox-active aromatic molecules that play roles in biological electron-transfer processes, the quinones, have been formed in numerous laboratory simulations of UV-photolyzed interstellar and planetary ices containing PAHs.^{22,23} Anthrarufin is a partially oxidized form of 9,10-anthraquinone, which, along with other anthracene ketones, has been found in the Murchison meteorite.^{24,25} These ketones were formed in the laboratory when anthracene was oxidized by exposure to UV radiation in H_2O ice under simulated astrophysical conditions.²²

The selected mineral substrates, including chromium oxide (Cr_2O_3) and manganese oxide (MnO), have been found in carbonaceous meteorites²⁶ and offer clues about the evolution of the solar nebula. Cr_2O_3 is a semiconductor, band gap ~ 5 eV,²⁷ that exhibits photocatalytic activity. It is believed to be one of the first major minerals to condense in the solar nebula and to form grains and nucleation points.²⁸ Iron oxide minerals, especially magnetite (Fe_3O_4) and hematite ($\alpha\text{-Fe}_2\text{O}_3$), are found in the martian regolith and dust.²⁹ Magnetite displays semimetallic conductivity³⁰ in addition to its magnetic properties, while Fe_2O_3 has a band gap of about 2 eV and is a well-studied photocatalyst.³¹ From an astrobiology perspective, Fe_2O_3 represents a promising potential catalyst for organic photoreactions. Nanosized iron oxide dust particles were discovered on Mars by the Mars Express OMEGA instrument in combination with Mars Exploration rover data sets.³² Dust nanoparticles have a high surface-to-volume ratio and can be exceptionally mobile, both important factors for catalytic activity.

Titanium dioxide (TiO_2) is present on the inner planets of the solar system;³³ it is a semiconductor with a 3 eV band gap and is well known for its photocatalytic activity, including the photoelectrolysis of water.³⁴ On Mars, titanium dioxide may likely be one of multiple important inorganic (photo)oxidants that play a role in the in situ degradation of organics,^{35,36} notwithstanding the discovery by the Mars Phoenix Mission of a significant presence of perchlorates.³⁷

As a mineral, iron sulfide (FeS_2 , pyrite) is found on Earth as a major component in organic-matter-bearing marine sediments. The Stardust Mission's captured cometary sample included

submicrometer Fe–Ni sulfide and Fe–Ni metal particles as well as olivine and pyroxene minerals with sizes $>1 \mu\text{m}$.^{38–40}

Silicon dioxide and silicates represent one of the most abundant forms of silicon in the universe in the form of cosmic dust.^{41,42} Olivine, $(\text{Mg}^{2+}_{1-x}\text{Fe}^{2+}_x)_2\text{SiO}_4$, is another class of candidate OREOCube inorganic samples, namely, metal-rich silicates. Forsterite (Mg_2SiO_4) and fayalite (Fe_2SiO_4) are the two stoichiometry-end-members of the olivine class. Apart from its occurrence on planetary bodies such as the Moon and Mars,⁴³ grains of forsterite have been found in cometary samples returned by the Stardust Mission.⁴⁴

In preparation for the OREOCube experiment, we performed laboratory characterization of anthrarufin and its photochemical degradation. We show here preflight results from UV-photolysis experiments performed on thin films of anthrarufin while in contact with iron oxides as an example for organic/inorganic thin film interactions relevant to astrochemistry and astrobiology.

1.4. OREOCube ISS Implementation. Since the principal measurement tool of OREOCube is UV–vis–NIR spectroscopy, preflight sample characterization is crucial in documenting any chemical changes that may occur between sample preparation and the initiation of space exposure as well as ensuring accurate in situ sample measurement on the ISS.⁴⁵ A typical OREOCube sample consists of optically thin films with spectral features in the 240–800 nm wavelength range. To study the most informative photochemical changes, ground-based studies have been used to determine which thin-film materials are likely to show significant changes in structure, as measured by UV–vis–NIR spectroscopy, and whether possible photoproducts can be measured in situ. Since the OREOCube samples will be retrieved at the end of the 12- to 18-month exposure experiment and returned to Earth, postflight analysis will be possible, allowing the use of complementary analytical techniques to further characterize the samples.

The suitability of a given organic thin film for the OREOCube experiment is based on its UV–visible spectrum as well as its anticipated stability/reactivity over the full duration of the OREOCube mission. Inorganic thin-film materials are being selected initially on the basis of their astrobiological and astrochemical relevance. They have been deemed suitable for flight experiments if they can be readily prepared in thin-film form on one or more of the available window materials and if their transmittance characteristics permit the recognition of the UV–vis features of the organic thin film following its deposition as an overlayer.

Current plans call for the ISS deployment of three independent sets of samples for each type of organic-on-inorganic thin film. Film duplicates for independence and system-level redundancy will be exposed to space radiation, including direct solar illumination outside the ISS, while the third set of samples will be kept nearby in the dark to serve as a control.

2. EXPERIMENTAL DETAILS

2.1. OREOCube Science Platform. The OREOCube platform (Figure 1a) is composed of a pair of 10 cm cubes each containing a compact UV–vis–NIR spectrometer, a 24-cell sample carousel, and the collection optics, motor, mechanical structure, and electronics that allow periodic collection, storage, and transfer of optical transmission spectra from each of the organic thin-film samples using the Sun as the light source.

The spaceflight lineage of the OREOCube spectrometer (from Aurora Design and Technology, an affiliate of Draper Laboratory,

Cambridge MA, USA) includes both O/OREOS-SEVO and the UV-visible spectrometer on the Lunar Crater Observing and Sensing Satellite (LCROSS) that impacted the Moon in October of 2009.⁴⁶ The key specifications of the OREOCube payload are shown in Table 3. To measure each sample spectrum, a carousel, driven by a stepper

Table 3. OREOCube Key Specifications

feature	specification(s)
form factor	two identical 1U (10 cm) cubes
number of samples	40 plus 8 references
solar exposure wavelengths	~120–7500 nm
exposure time	~12 months in ISS orbit
spectrometer wavelength range	200–1000 nm
spectral resolution	1–2 nm
detector integration time	100 ms (adjustable)
on-board spectral averaging	≥16× (adjustable)
temperature range of samples	–20 to +30 °C (calculated)
sample temperature sensors	two pyrometers on each carousel
detector temperature sensors	two ASICs for each spectrometer
spectral acquisition criterion	Sun cone angle < ±35° off-normal

motor, rotates the sample cell over a collection optics assembly that focuses collimated transmitted sunlight into an all-silica optical fiber linked to the spectrometer (Figure 1b). A poly(tetrafluoroethylene) optical diffuser broadens the acceptance angle of the optical system to more than 10° from normal solar incidence while ensuring that the measured portion of the organic film is uniformly illuminated. A variable-density filter in front of the linear charge-coupled-device (CCD) array detectors and a UV-response-enhancing coating on the CCDs combine to enhance the relative sensitivity in the NIR and UV ranges where solar intensity is low. Integrated circuit and optical pyrometer temperature sensors periodically monitor the respective temperatures of the spectrometer and sample carousel.

2.2. OREOCube Samples and Sample Cells. The OREOCube experiments will use combinations of the materials listed in Tables 1 and 2 to examine the effects of inorganic/organic interfaces that may

play an important role in the (photo)chemistry of organics on interplanetary/interstellar dust grains, comets, and other large- and small-body surfaces. Because surface morphology and particle size can have large impacts on photochemical processes, the inorganic materials (Table 2) are first deposited as either continuous or discontinuous optically thin films. Typically, discontinuous films are composed of high-surface-area islands or clusters that can display different photochemical properties than continuous films. Control of P_{O_2} and P_{H_2O} in the deposition chamber along with postdeposition processing allows the extent of inorganic oxide formation to be controlled for metals. A given organic thin film is then thermally deposited by vacuum sublimation on top of the inorganic thin film using a separate high-vacuum chamber enclosed in a glovebox. The film thickness, which varies by sample type, is monitored during deposition using a quartz crystal microbalance (QCM). The desired final sample thickness depends on the UV or visible light absorbance: generally, a range of 0.3 to 0.6 absorbance units (AU), i.e., 50–25% transmittance, is chosen for the primary absorption or the absorption feature of greatest interest.

OREOCube sample cells (Figure 1b,c) are constructed from a stainless-steel spacer ring (9 mm outer diameter × 4.5 mm inner diameter × 3 mm height) and MgF_2 , sapphire, or fused silica windows. The sample cell headspace gas composition, including the partial pressure of water vapor, is established by hermetically sealing the sample cells at room temperature in a controlled-atmosphere glovebox.¹⁶ The water content in the reaction cell during radiolysis can be controlled by directly binding water in the sample matrix or by controlling P_{H_2O} in the sample cell by including a hydrated salt retained on the side wall of the reaction cell as demonstrated for O/OREOS-SEVO.¹⁶ Spectra of cells with no sample and direct solar spectra (not passing through any cell prior to entering the collection optics) serve as spectral blanks and references.

The sample cells can be mounted with the sample window on the top side (Sun-facing) or bottom side (spectrometer-facing) of the carousel. The choice of sample window material (MgF_2 , Al_2O_3 , or SiO_2) and sample window mounting position depend on the film adhesion properties, window wavelength transmission, and desired

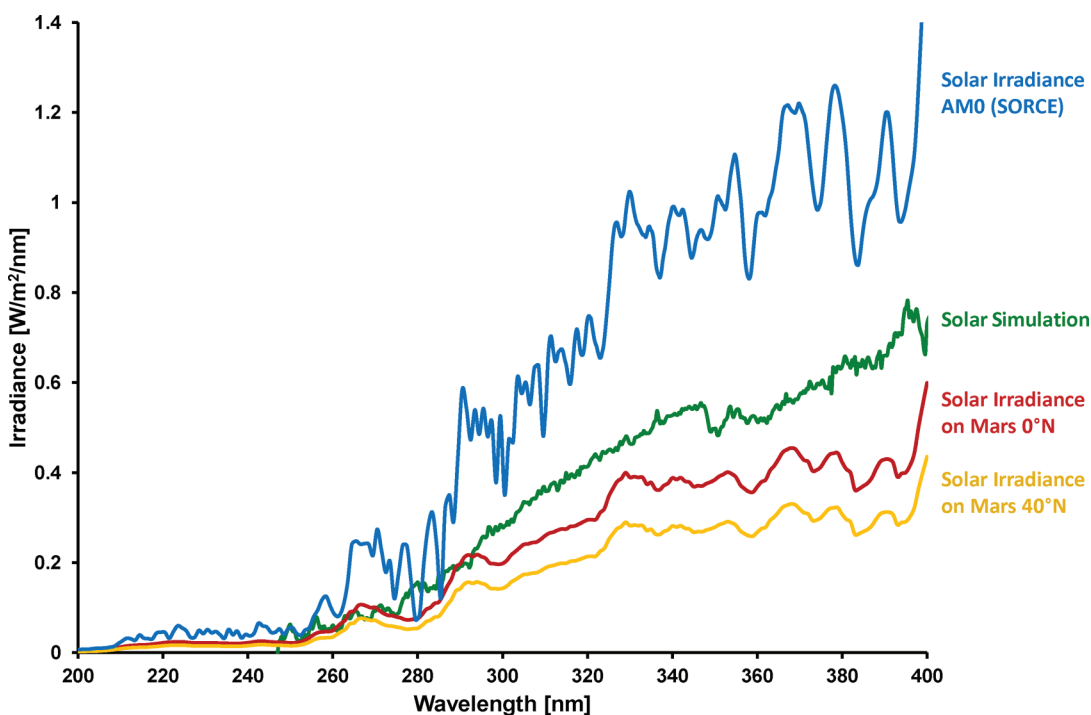


Figure 2. Irradiance of solar simulation experiment (green) in comparison to AM0 solar irradiance (blue, solar irradiance data from May 13, 2010 as recorded by the SORCE mission⁴⁹ at ISS) and computed irradiance on Mars at two latitudes, 0° N (red) and 40° N (yellow).⁴⁸

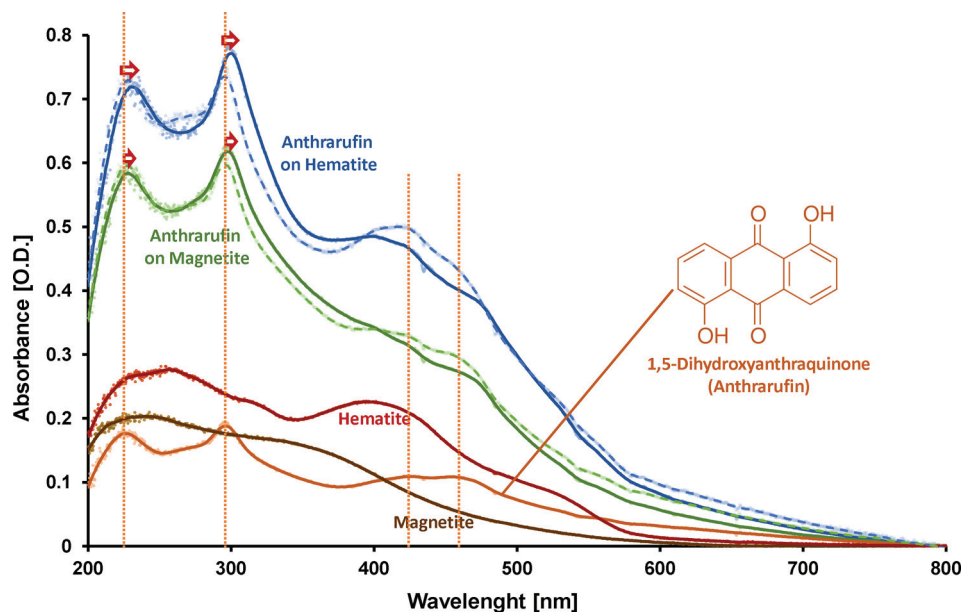


Figure 3. UV–visible spectra of anthrarufin (51 nm thick) on iron oxide (prepared by oxidizing 2 nm of Fe to yield ~ 4 nm of hematite or magnetite) in a bilayer arrangement as well as anthrarufin on fused silica and each type of iron oxide on bare fused silica. Dashed green and blue lines show mathematically added and scaled spectra of anthrarufin plus the respective iron oxide spectrum. The scaling factor was determined by the least-squares fitting of superimposed spectra to the original bilayer composite spectra. Orange dashed vertical lines show positions of main spectral features of anthrarufin. Red arrows indicate peak shifts toward longer wavelengths for anthrarufin on magnetite and on hematite.

radiation path relative to the inorganic/organic film structure. After the deposition of an optically thin inorganic sample (Table 2), the organic thin film sample (Table 1) is deposited on top of the inorganic. Thus, for cells with the sample window mounted on the top side, after passing through the sample window, photons impinge on the inorganic film before interacting with the organic film. Conversely, for cells with sample windows mounted on the bottom side of the carousel, photons first pass through the uncoated window and impinge on the organic film (which is deposited over the inorganic film).

2.3. Film Preparation and Laboratory UV Exposure. Preflight laboratory experiments were performed with a subset of inorganic and organic thin-film candidates. We present below the results from experiments conducted with iron oxide thin films in combination with a thin film of the quinone anthrarufin. Iron oxide films were prepared for laboratory studies by the physical vapor deposition of metallic iron (99.99%, Sigma-Aldrich, St. Louis, MO, USA) in a high-vacuum deposition chamber ($\sim 1 \times 10^{-4}$ Pa). After deposition, the films were converted to magnetite or hematite by heating for 4 h in the presence of an oxygen atmosphere at 175 or 575 $^{\circ}\text{C}$, respectively.⁴⁷ The thickness of the iron films prior to oxidation was 2 nm, hence stoichiometries and (bulk) densities dictate that the thickness of both magnetite and hematite films is ~ 4 nm as a result of the quantitative oxidation of the Fe. Anthrarufin thin films (51 nm) were deposited as described above either on uncoated fused silica (SiO_2) or on top of hematite or magnetite deposited on SiO_2 . Anthrarufin (Sigma-Aldrich) was prepurified by heating under vacuum prior to film deposition.

UV exposure was performed using a Hanovia 1000 W Xe arc lamp with an IR water filter to prevent sample heating. The inorganic/organic films were exposed, as a single lot, in a sample chamber with a Suprasil fused silica optical port. Sample windows were positioned with the films facing the light source so that light first passed through the organic film, then the inorganic film, and finally the fused silica window. An 800 Pa CO_2 (99.99%) atmosphere, with a mass-flow-controlled 0.15 cm^3/min flow rate, was maintained using an oil-free diaphragm pump. The dew point was held between -50 and -60 $^{\circ}\text{C}$ ($P_{\text{H}_2\text{O}} \approx 2\text{--}6$ Pa). To obtain UV–vis spectra, our laboratory setup required that the samples be removed temporarily from the CO_2 -purged chamber and exposed to laboratory air; they were then returned to the CO_2 chamber to continue irradiation. The overall objective of these experiments was to examine UV photolysis under

Mars-relevant conditions (i.e., Mars P_{CO_2} and $P_{\text{H}_2\text{O}}$ in combination with iron oxide interactions) as selection criteria for OREOCube ISS samples.

2.4. Characterization of the UV Lamp with Comparison to Mars and ISS Solar Flux. Figure 2 shows the UV output of the laboratory Xe lamp over the range of 180 to 400 nm compared to the UV solar flux in Mars' equatorial regions (0 and 40°) as modeled by Patel et al.,⁴⁸ along with the expected flux for the OREOCube experiment at the ISS.⁴⁹ The integrated (200–400 nm) UV flux during the laboratory exposures was 62 ± 0.5 W/m^2 compared to ~ 44 W/m^2 for Mars at the equator and ~ 108 W/m^2 for an AM0 solar spectrum outside Earth's atmosphere. The solar simulator has no substantial flux below 247 nm.

3. LABORATORY RESULTS AND DISCUSSION

3.1. Spectra of As-Deposited Films. The optical transmission characteristics of iron oxide thin films were determined to evaluate their suitability for the OREOCube flight experiments. They were determined to be consistent with those previously reported in the literature and to have sufficient transmission for the space experiment (see Figure 3).⁵⁰ The two main peaks (~ 250 and ~ 400 nm) in the UV–vis spectrum of hematite are attributed to charge-transfer bands, resulting from electron transfer from the O 2p to Fe 3d orbital. The shoulder at ~ 525 nm and weaker features between ~ 450 and ~ 550 nm are attributed to ligand-field transitions.^{51–53} UV–vis spectra of anthrarufin show characteristic peaks at 230 nm as well as at 295 nm.¹⁸ A broader peak between 400 and 490 nm with subfeatures at 425 and 460 nm is also visible. Absorption bands at 230 nm (including a small shoulder at 272 nm) and in the 400–490 nm wavelength range are attributed to $\pi \rightarrow \pi^*$, HOMO to LUMO (highest occupied to lowest unoccupied molecular orbital), transitions and can be assigned to the benzenoid and quinonoid systems of the molecule. These transitions are oriented along the long axis of the molecule⁵⁴ and are common spectral features of anthraquinone compounds.⁵⁵ The band at 295 nm also stems from $\pi \rightarrow \pi^*$

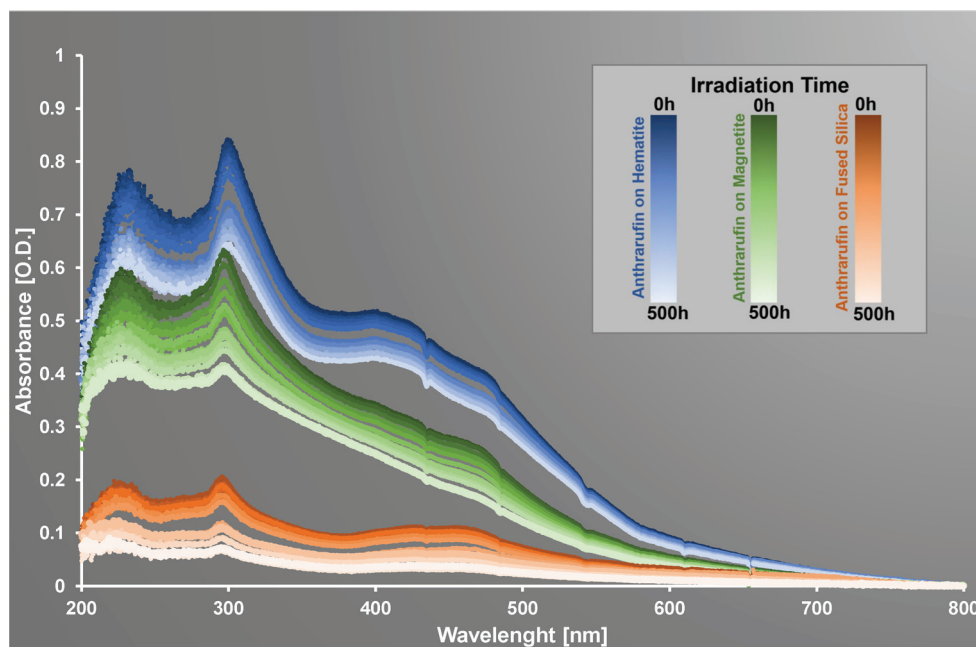


Figure 4. Time-dependent UV–visible spectra of a bilayer thin film composed of anthraruflin on iron oxide (magnetite (green) and hematite (blue)) as well as anthraruflin alone (orange), all on fused silica substrates. Color shades from dark to light illustrate the qualitative spectral change from 0 to 500 h of simulated solar irradiation at intensities typical of the surface of Mars.

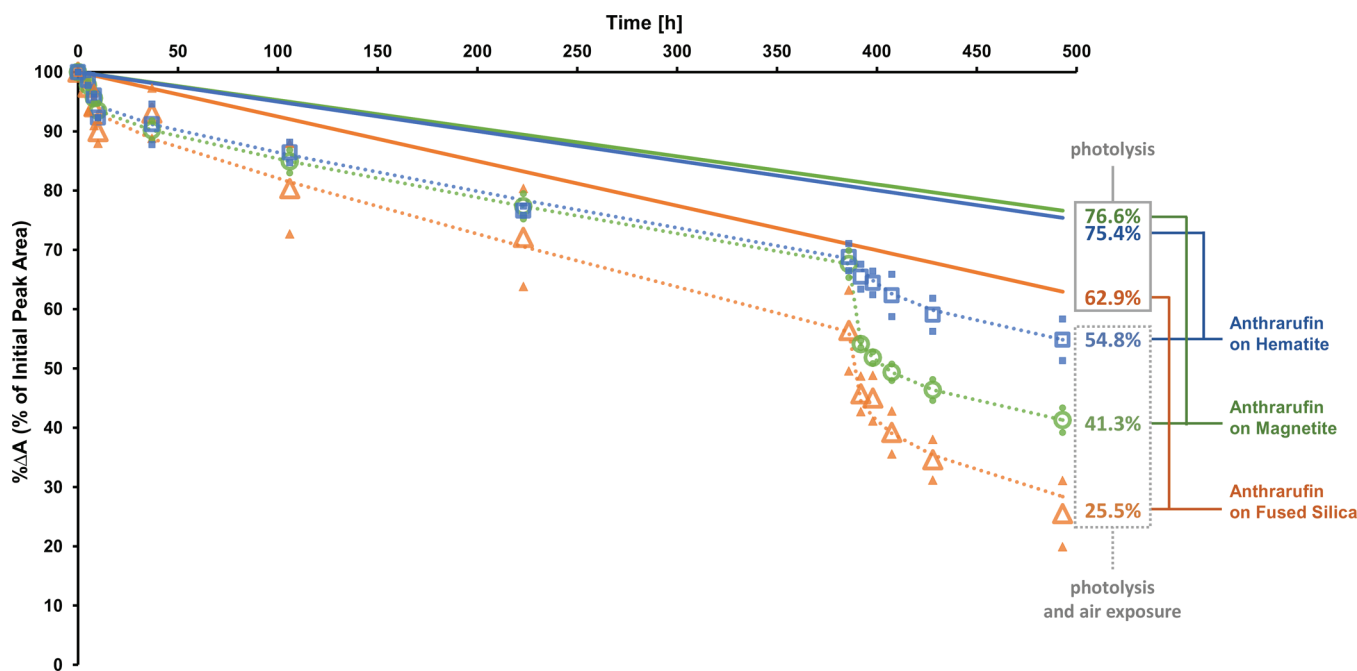


Figure 5. UV–visible spectral changes of anthraruflin films on fused silica (orange triangles) and with iron oxide (magnetite, green circles; hematite, blue squares) underlying films represented by relative changes in peak area compared to the initial area of the anthraruflin main peak near 300 nm as a function of the simulated solar exposure time. Small filled symbols represent two independent samples of a given type; open symbols are mean values of those two samples. Averaged data are least-squares fit to a model (dotted curves, see eq 1) that accounts for a steady-state photolysis rate whenever the samples are illuminated plus a step change in absorbance each time the samples are exposed (transiently) to air. Solid straight lines represent calculated changes in the percentage peak area derived from the first term of the model (eq 1), which takes into account only the linear-with-time steady-state photolysis reaction and not the observed step degradation caused by each air exposure.

transitions with a major contribution from the $-\text{OH}$ substituents; it is directed along the short axis of the molecule.⁵⁴

As shown in Figure 3, the absorptivities of the anthraruflin bands for the films supported on hematite and magnetite are, in the 200–500 nm wavelength region, up to 3 times larger than

those of anthraruflin films, of the same thickness, on fused silica. Nonetheless, the spectral features can be clearly discerned in all samples. Figure 3 also shows the spectra of anthraruflin on silica scaled and summed with both the hematite and magnetite spectra, compared to the spectra of the multilayer films (all supported by fused silica substrates). The coadded and scaled

anthrarufin-plus-iron oxide spectra have noticeable differences from the actual spectra of the composite thin films. Band positions and relative intensities for anthrarufin appear altered, with the most obvious alterations being in the spectrum of anthrarufin on hematite. For instance, the main anthrarufin bands at ~ 230 and 295 nm exhibit small shifts toward longer wavelength, ~ 2 nm for anthrarufin on magnetite and ~ 4 nm for anthrarufin on hematite, relative to anthrarufin on a pure SiO_2 surface.

The spectral differences among the three sample types occur in overall absorptivity as well as peak shape and position. The most prominent observed difference between anthrarufin on fused silica and anthrarufin on iron oxides is the increased (by more than a factor of 2) overall absorptivity of the latter. It is known that iron oxides form charge-transfer complexes with organic molecules that can result in increased molar absorptivity.⁵⁶ Similar effects have been observed with fluorophores, for which the fluorescence intensity increases due to close-proximity interactions with metal or semiconducting surfaces or nanoparticles.⁵⁷ While we cannot entirely rule out thin-film optical effects that could enhance the apparent absorptivity of anthrarufin,⁵⁸ peak shifts, as observed for anthrarufin on magnetite and hematite, have been reported to be caused by the conjugation between chromophores and substrates⁵⁶ and therefore indicate, in this case, small modifications in their molecular orbital energy levels as well as absorptivities.⁵⁹

3.2. UV-Visible Photolysis of One- and Two-Layer Films. Both types of iron oxide thin films were subjected to simulated solar exposure for 493 h, corresponding to a total UV dose (200–400 nm) of ~ 110 MJ/m². No spectral change in either hematite ($\alpha\text{-Fe}_2\text{O}_3$) or magnetite (Fe_3O_4) was observed over the duration of this irradiation.

UV-vis spectra of anthrarufin on bare fused silica substrates as well as on magnetite and hematite films supported on fused silica were recorded as a function of time over a period of nearly 500 h of simulated solar exposure. Figure 4 illustrates, qualitatively, the general time-dependent spectral changes in the thin-film absorbance spectra for anthrarufin and anthrarufin/iron oxide film bilayers. A more quantitative analysis follows in the context of reaction rates.

In order to analyze in greater detail the kinetic behavior of anthrarufin with and without underlying iron oxide films, spectral changes were compared by means of integrated absorbance peak areas and absorbance peak heights as a function of time. Peak area was found to be the more robust parameter for monitoring anthrarufin degradation rates under simulated solar exposure. Relative changes in the peak area of the main anthrarufin feature near 300 nm vs time are shown in Figure 5. Data from two independent sample sets for each anthrarufin/iron oxide combination, as well as for anthrarufin alone, are displayed.

To understand and explain the complex kinetic behavior shown in Figure 5, averaged data (open symbols) of the two samples per material type were fitted to a two-parameter model that describes the steady-state photolysis of the organic thin film whenever the samples are illuminated as well as a step effect that we ascribe to each of the multiple exposures of the samples to air over the course of the measurement. (The experimental setup does not permit the collection of UV-vis spectra in situ under the CO_2 atmosphere; thus, samples were briefly exposed to air each time spectra were recorded.) We postulated such a model because the time dependence of the

absorbance data of Figure 5 appears to indicate larger amounts of photolysis when air exposure is more frequent. This suggested that a second parameter in addition to the steady-state photolysis term would be required to account for the effect of air exposure. The postulated relationship among the change in integrated normalized absorbance peak area at 300 nm, ΔA_{300} , cumulative exposure time, t , steady-state photolysis rate, r , and total number of air exposures, n , is modeled as

$$\Delta A_{300}(n, t) = rt + n\Delta a + \Delta a_{\text{setup}}(t) \quad (1)$$

where Δa is the incremental absorbance step change associated with each air exposure, r is the (constant) rate of absorbance change due to photolysis whenever the samples are illuminated (independent of the number of previous air exposures), and Δa_{setup} is a one-time step change in absorbance that occurred due to an optical alignment issue at $t = 386$ h ($\Delta a_{\text{setup}} = 0$ for $t < 386$ h; Δa_{setup} is a constant specific to each sample for all $t > 386$ h with $\Delta a_{\text{setup}} < 0.06$ for all samples). The values of parameters Δa and r were determined by linear least-squares fitting.

The results in Figure 5 are reasonably well fit by the model (smooth dotted lines). The comparatively more rapid photolysis subsequent to each air exposure is consistent with a process that involves a component of air, presumably either H_2O or O_2 , which would have to react with or chemisorb on (in) the organic film during air exposure and either cause an immediate loss of absorbance or remain in/on the film long enough to cause accelerated photolysis once illumination resumed. Both species are also present, albeit at much lower concentrations, in the high-purity CO_2 in which the photolysis was conducted ($P_{\text{H}_2\text{O}} \approx 2\text{--}6$ Pa; $P_{\text{O}_2} < 0.5$ Pa). Thus, a single mechanism and rate-limiting species could be responsible for both steady-state photolysis and rapid, steplike changes in absorbance each time the films were photolyzed just after exposure to laboratory air.

Significant kinetic differences are observed in Figure 5 as a function of time and the identities of the photolyzed samples. The initial rates of change in all samples in the 0–10 h time frame are strongly influenced by the effects of multiple air exposure. Major differences during this period between film types are difficult to determine due to intersample variability. The rapid initial degradation is followed, beginning at $t \approx 10$ h, by a slower overall rate of change for all three film types due to less frequent exposure to air. From $t = 10\text{--}386$ h of irradiation, steady-state UV photolysis dominates the degradation process. After $t = 386$ h, measurements were made again more frequently, hence there was more frequent exposure of the samples to laboratory air, and a noticeable increase in the degradation rate is clearly visible for all three film types. (It was this observation that led us to the model described by eq 1.)

As noted in section 3.1 and shown in Figure 3, the peak area for the same thickness of anthrarufin depends strongly on the underlying substrate. Therefore, in order to illustrate the relative rates of degradation of anthrarufin with and without underlying iron oxide films, the data of Figure 5 are plotted as the percent change in integrated peak areas relative to the initial unphotolyzed peak area for each sample. Also shown in Figure 5 (solid lines) are linear fits, based solely on the first term of eq 1 (rt), that represent the modeled photolysis of anthrarufin absorbance on fused silica, magnetite, and hematite without the effects of air exposure. Overall, our data show that anthrarufin on silica is photolyzed more rapidly than films with an iron

oxide substrate; anthrarufin on fused silica degrades about 1.2 times faster than anthrarufin on iron oxide substrates when only the rate of photolysis during the periods without air exposure is considered.

The photodegradation of anthraquinones has been explained via a two-step process by Ossowski and co-workers:⁶⁰ an electron-capture process is followed by oxygen reactions with the semiquinone anion radical thus formed. Like other metal oxides, the iron oxide layers could act as an electron buffer,⁵⁹ quenching the formation of the semiquinone anion radical and therefore slowing the degradation process. The interactions of anthrarufin with its iron oxide substrates, apparent in the band shifts of Figure 3, are consistent with this photolysis protection mechanism. (The enhanced absorptivity of the iron oxide-supported films is likely additional evidence of this interaction, although it could result in part from thin-film optical effects.⁵⁸)

The experiments reported here demonstrate intriguing differences in kinetics for anthrarufin thin films as a consequence of their underlying substrates. The results of Figure 5 highlight the power of time-resolved spectral measurements that record not only starting and ending points but also dynamic changes and alteration rates. The ground-based experimental data presented here were recorded at varying intervals by manual procedures. Air exposure of the samples during UV–vis measurements was unavoidable for our laboratory setup, but even this constraint resulted in an interesting kinetic effect that differentiates the three sample types, as revealed by the analysis of Figure 5. For OREOCube on the ISS, in situ spectral measurements will be obtained under space radiation environment conditions (UV and particle) without intervening air exposures; the experiment will be fully autonomous and remotely controlled.

4. CONCLUSIONS AND SUMMARY

The capability to measure in situ the changes in samples exposed to space radiation as a function of time in low Earth orbit confers significant advantages relative to laboratory simulators and more basic ISS exposure facilities for which sample measurements are made on Earth prior to and at the conclusion of a space mission. OREOCube will be the first of a new generation of experiments to combine both autonomous and in situ measurement technologies to characterize organic and mineral thin films, individually and as layered composites, on the ISS with the advantages of postexposure sample return allowing further analyses.

In preparation for the OREOCube spaceflight experiment aboard ISS (tentative launch schedule 2015), preliminary ground-based research on the photochemistry of anthrarufin in contact with hematite and magnetite thin films shows the practicality of the study of bilayer thin films using the methodology outlined here. Anthrarufin and iron oxide thin films interact strongly in terms of electronic structure, apparent in altered spectral features and overall absorptivity relative to anthrarufin supported on fused silica substrates. Our experimental results show that the photolytic degradation of anthrarufin on iron oxides is comparatively slower than that of anthrarufin on fused silica substrates. Hence, instead of a catalytic effect, iron oxides display a photolysis-inhibiting effect, which is most likely due to their electron-buffering capability. This effect decelerates the oxidation of anthrarufin by quenching free-electron production and anion formation. The detailed kinetic results obtained and analyzed highlight the potential of time-resolved in situ measurements to elucidate

mechanistic photodegradation details for exposure experiments in space. The interactions of organic molecules with inorganic surfaces and their potential catalytic and/or inhibiting action are of great interest to the astrochemistry and astrobiology communities. Coupling such experiments with sample return and in-depth analysis in terrestrial laboratories to further elucidate the degradation end products of thin film photolysis will amplify the insight gained from such space-based exposure studies.

AUTHOR INFORMATION

Corresponding Authors

*E-mail: a.elsaesser@umail.leidenuniv.nl

*E-mail: richard.c.quinn@nasa.gov

*E-mail: ajricco@stanford.edu

Author Contributions

The manuscript was written through the contributions of all authors. All authors have given approval to the final version of the manuscript.

Notes

The authors declare no competing financial interest.

ACKNOWLEDGMENTS

We gratefully acknowledge helpful discussions regarding thin-film optical effects with Dr. Nathan Bramall of Los Gatos Research, Inc. The European participation in OREOCube is funded by The Netherlands Organisation for Scientific Research (Evolution of organics in space: OREOCube in situ spectroscopy). OREOCube was proposed to the International Research Announcement for Research in Space Life Sciences (ILSRA 2009) and selected for Definition Phase by the European Space Agency (ESA). U.S. participation in OREOCube is funded by the NASA Astrobiology Science and Technology Instrument Development (ASTID) program. We thank Dr. Monika Kress (San Jose State University) and Dr. Cynthia B. Phillips (SETI Institute) for providing partial funding for A.B. and Y.K.C. through the Undergraduate Research at SETI Institute in Astrobiology (URSA) Program (a NASA Education and Public Outreach in Earth and Space Science program award). Partial funding for J.A. was provided by National Science Foundation award no. AST-0847170, a PAARE grant for the California-Arizona Minority Partnership for Astronomy Research and Education (Dr. Alex Rudolph, Director).

ABBREVIATIONS

AMO, air mass zero; AU, absorbance unit; CCD, charge-coupled device; ESA, European Space Agency; FeTTPCl, iron(III)-5,10,15,20-tetraphenyl-21H,23H-porphine chloride; HOMO, highest occupied molecular orbital; IR, infrared; ISS, International Space Station; LUMO, lowest unoccupied molecular orbital; NASA, National Aeronautics and Space Administration; NIR, near-infrared; O/OREOS, Organism/ORganic Exposure to Orbital Stresses; OREOCube, Organics Exposure in Orbit cube; PAH, polycyclic aromatic hydrocarbon; QCM, quartz crystal microbalance; SETI, Search for Extraterrestrial Intelligence; SEVO, Space Environment Viability of Organics; UV, ultraviolet; vis, visible

REFERENCES

(1) Ehrenfreund, P.; Charnley, S. B. *Organic Molecules in the Interstellar Medium, Comets, and Meteorites: A Voyage from Dark*

Clouds to the Early Earth. *Annu. Rev. Astron. Astrophys.* **2000**, *38*, 427–483.

(2) Henning, T.; Salama, F. Carbon in the Universe. *Science* **1998**, *282*, 2204–2210.

(3) Tielens, A. The molecular universe. *Rev. Mod. Phys.* **2013**, *85*, 1021.

(4) Gomes, R.; Levison, H. F.; Tsiganis, K.; Morbidelli, A. Origin of the cataclysmic Late Heavy Bombardment period of the terrestrial planets. *Nature* **2005**, *435*, 466–9.

(5) Walsh, K. J.; Morbidelli, A.; Raymond, S. N.; O'Brien, D. P.; Mandell, A. M. Populating the asteroid belt from two parent source regions due to the migration of giant planets—"The Grand Tack. *Meteorit. Planet. Sci.* **2012**, *47*, 1941–1947.

(6) Chyba, C.; Sagan, C. Endogenous production, exogenous delivery and impact-shock synthesis of organic molecules: an inventory for the origins of life. *Nature* **1992**, *355*, 125–132.

(7) Ehrenfreund, P.; Irvine, W.; Becker, L.; Blank, J.; Brucato, J. R.; Colangeli, L.; Derenne, S.; Despois, D.; Dutrey, A.; Fraaije, H.; Lazcano, A.; Owen, T.; Robert, F. International Space Science Institute, I-T. Astrophysical and astrochemical insights into the origin of life. *Rep. Prog. Phys.* **2002**, *65*, 1427–1487.

(8) Cronin, J. R.; Chang, S. Organic Matter in Meteorites: Molecular and Isotopic Analyses of the Murchison Meteorite. *The Chemistry of Life's Origins*; Springer, 1993; pp 209–258.

(9) Botta, O.; Bada, J. L. Extraterrestrial organic compounds in meteorites. *Surv. Geophys.* **2002**, *23*, 411–467.

(10) Ehrenfreund, P.; Sephton, M. A. Carbon molecules in space: from astrochemistry to astrobiology. *Faraday Discuss.* **2006**, *133*, 277–288.

(11) Guan, Y. Y.; Fray, N.; Coll, P.; Macari, F.; Chaput, D.; Raulin, F.; Cottin, H. UVolution: compared photochemistry of prebiotic organic compounds in low Earth orbit and in the laboratory. *Planet. Space Sci.* **2010**, *58*, 1327–1346.

(12) Cook, A. M.; Mattioda, A. L.; Quinn, R. C.; Ricco, A. J.; Ehrenfreund, P.; Bramall, N. E.; Minelli, G.; Quigley, E.; Walker, R.; Walker, R. SEVO on the Ground: Design of a Laboratory Solar Simulation in Support of the O/OREOS Mission. *Astrophys. J. Suppl. Ser.* **2014**, *210*, 15.

(13) Horneck, G.; Klaus, D. M.; Mancinelli, R. L. Space microbiology. *Microbiol. Mol. Biol. Rev.* **2010**, *74*, 121–56.

(14) Rabbow, E.; Rettberg, P.; Barczyk, S.; Bohmeier, M.; Parpart, A.; Panitz, C.; Horneck, G.; von Heise-Rotenburg, R.; Hoppenbrouwers, T.; Willnecker, R.; Baglioni, P.; Demets, R.; Dettmann, J.; Reitz, G. EXPOSE-E: an ESA astrobiology mission 1.5 years in space. *Astrobiol. J.* **2012**, *12*, 374–86.

(15) Ehrenfreund, P.; Ruitkamp, R.; Peeters, Z.; Foing, B.; Salama, F.; Martins, Z. The ORGANICS experiment on BIOPAN V: UV and space exposure of aromatic compounds. *Planet. Space Sci.* **2007**, *55*, 383–400.

(16) Bramall, N. E.; Quinn, R.; Mattioda, A.; Bryson, K.; Chittenden, J. D.; Cook, A.; Taylor, C.; Minelli, G.; Ehrenfreund, P.; Ricco, A. J.; Squires, D.; Santos, O.; Friedericks, C.; Landis, D.; Jones, N. C.; Salama, F.; Allamandola, L. J.; Hoffmann, S. V. The development of the Space Environment Viability of Organics (SEVO) experiment aboard the Organism/Organic Exposure to Orbital Stresses (O/OREOS) satellite. *Planet. Space Sci.* **2012**, *60*, 121–130.

(17) Ehrenfreund, P.; Ricco, A. J.; Squires, D.; Kitts, C.; Agasid, E.; Bramall, N.; Bryson, K.; Chittenden, J.; Conley, C.; Cook, A.; Mancinelli, R.; Mattioda, A.; Nicholson, W.; Quinn, R.; Santos, O.; Tahu, G.; Voytek, M.; Beasley, C.; Bica, L.; Diaz-Aguado, M.; Friedericks, C.; Henschke, M.; Landis, D.; Luzzi, E.; Ly, D.; Mai, N.; Minelli, G.; McIntyre, M.; Neumann, M.; Parra, M.; Piccini, M.; Rasay, R.; Ricks, R.; Schooley, A.; Stackpole, E.; Timucin, L.; Yost, B.; Young, A. The O/OREOS mission—Astrobiology in low Earth orbit. *Acta Astronaut.* **2014**, *93*, 501–508.

(18) Mattioda, A.; Cook, A.; Ehrenfreund, P.; Quinn, R.; Ricco, A. J.; Squires, D.; Bramall, N.; Bryson, K.; Chittenden, J.; Minelli, G.; Agasid, E.; Allamandola, L.; Beasley, C.; Burton, R.; Defouw, G.; Diaz-Aguado, M.; Fonda, M.; Friedericks, C.; Kitts, C.; Landis, D.

McIntyre, M.; Neumann, M.; Rasay, M.; Ricks, R.; Salama, F.; Santos, O.; Schooley, A.; Yost, B.; Young, A. The O/OREOS mission: first science data from the space environment viability of organics (SEVO) payload. *Astrobiol. J.* **2012**, *12*, 841–53.

(19) Boersma, C.; Bregman, J. D.; Allamandola, L. J. Properties of Polycyclic Aromatic Hydrocarbons in the Northwest Photon Dominated Region of NGC 7023. I. PAH Size, Charge, Composition, and Structure Distribution. *Astrophys. J.* **2013**, *769*, 117.

(20) Sephton, M. A. Organic compounds in carbonaceous meteorites. *Nat. Prod. Rep.* **2002**, *19*, 292–311.

(21) Tielens, A. G. G. M. Interstellar Polycyclic Aromatic Hydrocarbon Molecules*. *Annu. Rev. Astron. Astrophys.* **2008**, *46*, 289–337.

(22) Ashbourn, S. F. M.; Elsil, J. E.; Dworkin, J. P.; Bernstein, M. P.; Sandford, S. A.; Allamandola, L. J. Ultraviolet photolysis of anthracene in H₂O interstellar ice analogs: Potential connection to meteoritic organics. *Meteorit. Planet. Sci.* **2007**, *42*, 2035–2041.

(23) Bernstein, M. P.; Sandford, S. A.; Allamandola, L. J.; Gillette, J. S.; Clemett, S. J.; Zare, R. N. UV irradiation of polycyclic aromatic hydrocarbons in ices: production of alcohols, quinones, and ethers. *Science* **1999**, *283*, 1135–8.

(24) Basile, B. P.; Middleditch, B. S.; Oró, J. Polycyclic aromatic hydrocarbons in the Murchison meteorite. *Org. Geochem.* **1984**, *5*, 211–216.

(25) Krishnamurthy, R.; Epstein, S.; Cronin, J. R.; Pizzarello, S.; Yuen, G. U. Isotopic and molecular analyses of hydrocarbons and monocarboxylic acids of the Murchison meteorite. *Geochim. Cosmochim. Acta* **1992**, *56*, 4045–4058.

(26) Rotaru, M.; Birck, J. L.; Allegre, C. J. Clues to early solar system history from chromium isotopes in carbonaceous chondrites. *Nature* **1992**, *358*, 465–470.

(27) Hong, S.; Kim, E.; Kim, D.-W.; Sung, T.-H.; No, K. On measurement of optical band gap of chromium oxide films containing both amorphous and crystalline phases. *J. Non-Cryst. Solids* **1997**, *221*, 245–254.

(28) Simon, S. B.; Davis, A. M.; Grossman, L.; McKeegan, K. D. A hibonite-corundum inclusion from Murchison: A first-generation condensate from the solar nebula. *Meteorit. Planet. Sci.* **2002**, *37*, 533–548.

(29) Blake, D. F.; Morris, R. V.; Kocurek, G.; Morrison, S. M.; Downs, R. T.; Bish, D.; Ming, D. W.; Edgett, K. S.; Rubin, D.; Goetz, W.; Madsen, M. B.; Sullivan, R.; Gellert, R.; Campbell, I.; Treiman, A. H.; McLennan, S. M.; Yen, A. S.; Grotzinger, J.; Vaniman, D. T.; Chipera, S. J.; Achilles, C. N.; Rampe, E. B.; Sumner, D.; Meslin, P.-Y.; Maurice, S.; Forni, O.; Gasnault, O.; Fisk, M.; Schmidt, M.; Mahaffy, P.; Leshin, L. A.; Glavin, D.; Steele, A.; Freissinet, C.; Navarro-González, R.; Yingst, R. A.; Kah, L. C.; Bridges, N.; Lewis, K. W.; Bristow, T. F.; Farmer, J. D.; Crisp, J. A.; Stolper, E. M.; Des Marais, D. J.; Sarrazin, P.; Team, M. S. Curiosity at Gale Crater, Mars: Characterization and Analysis of the Rocknest Sand Shadow. *Science* **2013**, *341*, 6153.

(30) Earnshaw, A.; Greenwood, N. *Chemistry of the Elements*, 2nd ed.; Butterworth-Heinemann: Oxford, U.K., 1997; p 1600.

(31) Schule, A.; Nieken, U.; Shekhah, O.; Ranke, W.; Schlogl, R.; Kolios, G. Styrene synthesis over iron oxide catalysts: from single crystal model system to real catalysts. *Phys. Chem. Chem. Phys.* **2007**, *9*, 3619–34.

(32) Arvidson, R. E.; Poulet, F.; Morris, R. V.; Bibring, J. P.; Bell, J. F.; Squyres, S. W.; Christensen, P. R.; Bellucci, G.; Gondet, B.; Ehlmann, B. L.; Farrand, W. H.; Fergason, R. L.; Golombek, M.; Griffes, J. L.; Grotzinger, J.; Guinness, E. A.; Herkenhoff, K. E.; Johnson, J. R.; Klingelhöfer, G.; Langevin, Y.; Ming, D.; Seelos, K.; Sullivan, R. J.; Ward, J. G.; Wiseman, S. M.; Wolff, M. Nature and origin of the hematite-bearing plains of Terra Meridiani based on analyses of orbital and Mars Exploration rover data sets. *J. Geophys. Res.: Planets* **2006**, *111*, E12S08.

(33) Davis, A. M. *Meteorites, Comets, and Planets: Treatise on Geochemistry*; Elsevier Science: Amsterdam, 2006; p 756.

- (34) Ni, M.; Leung, M. K. H.; Leung, D. Y. C.; Sumathy, K. A review and recent developments in photocatalytic water-splitting using for hydrogen production. *Renewable Sustainable Energy Rev.* **2007**, *11*, 401–425.
- (35) Quinn, R.; Zent, A. Peroxide-Modified Titanium Dioxide: a Chemical Analog of Putative Martian Soil Oxidants. *Origins Life Evol. Biospheres* **1999**, *29*, 59–72.
- (36) Chun, S. F.; Pang, K. D.; Cutts, J. A.; Ajello, J. M. Photocatalytic oxidation of organic compounds on Mars. *Nature* **1978**, *274*, 875–876.
- (37) Hecht, M.; Kounaves, S.; Quinn, R.; West, S.; Young, S.; Ming, D.; Catling, D.; Clark, B.; Boynton, W.; Hoffman, J. Detection of perchlorate and the soluble chemistry of martian soil at the Phoenix lander site. *Science* **2009**, *325*, 64–67.
- (38) Brownlee, D.; Tsou, P.; Aléon, J.; Alexander, C. M. O. D.; Araki, T.; Bajt, S.; Baratta, G. A.; Bastien, R.; Bland, P.; Bleuett, P.; Borg, J.; Bradley, J. P.; Brearley, A.; Brenker, F.; Brennan, S.; Bridges, J. C.; Browning, N. D.; Brucato, J. R.; Bullock, E.; Burchell, M. J.; Busemann, H.; Butterworth, A.; Chaussidon, M.; Chevront, A.; Chi, M.; Cintala, M. J.; Clark, B. C.; Clemett, S. J.; Cody, G.; Colangeli, L.; Cooper, G.; Cordier, P.; Daghlain, C.; Dai, Z.; D'Hendecourt, L.; Djouadi, Z.; Dominguez, G.; Duxbury, T.; Dworkin, J. P.; Ebel, D. S.; Economidou, T. E.; Fakra, S.; Fairey, S. A. J.; Fallon, S.; Ferrini, G.; Ferroir, T.; Fleckenstein, H.; Floss, C.; Flynn, G.; Franchi, I. A.; Fries, M.; Gainsforth, Z.; Gallien, J.-P.; Genge, M.; Gilles, M. K.; Gillet, P.; Gilmour, J.; Glavin, D. P.; Gounelle, M.; Grady, M. M.; Graham, G. A.; Grant, P. G.; Green, S. F.; Grossemy, F.; Grossman, L.; Grossman, J. N.; Guan, Y.; Hagiya, K.; Harvey, R.; Heck, P.; Herzog, G. F.; Hoppe, P.; Hörz, F.; Huth, J.; Hutcheon, I. D.; Ignatyev, K.; Ishii, H.; Ito, M.; Jacob, D.; Jacobsen, C.; Jacobsen, S.; Jones, S.; Joswiak, D.; Jurewicz, A.; Kearsley, A. T.; Keller, L. P.; Khodja, H.; Kilcoyne, A. L. D.; Kissel, J.; Krot, A.; Langenhorst, F.; Lanzirrotti, A.; Le, L.; Leshin, L. A.; Leitner, J.; Lemelle, L.; Leroux, H.; Liu, M.-C.; Luening, K.; Lyon, I.; MacPherson, G.; Marcus, M. A.; Marhas, K.; Marty, B.; Matrajt, G.; McKeegan, K.; Meibom, A.; Mennella, V.; Messenger, K.; Messenger, S.; Mikouchi, T.; Mostefaoui, S.; Nakamura, T.; Nakano, T.; Newville, M.; Nittler, L. R.; Ohnishi, I.; Ohsumi, K.; Okudaira, K.; Papanastassiou, D. A.; Palma, R.; Palumbo, M. E.; Pepin, R. O.; Perkins, D.; Perronnet, M.; Pianetta, P.; Rao, W.; Rietmeijer, F. J. M.; Robert, F.; Rost, D.; Rotundi, A.; Ryan, R.; Sandford, S. A.; Schwandt, C. S.; See, T. H.; Schlutter, D.; Sheffield-Parker, J.; Simionovici, A.; Simon, S.; Sitnitsky, I.; Snead, C. J.; Spencer, M. K.; Stadermann, F. J.; Steele, A.; Stephan, T.; Stroud, R.; Susini, J.; Sutton, S. R.; Suzuki, Y.; Taheri, M.; Taylor, S.; Teslich, N.; Tomeoka, K.; Tomioka, N.; Toppani, A.; Trigo-Rodríguez, J. M.; Troadec, D.; Tsuchiyama, A.; Tuzzolino, A. J.; Tyliszczak, T.; Uesugi, K.; Velbel, M.; Vellenga, J.; Vicenzi, E.; Vincze, L.; Warren, J.; Weber, I.; Weisberg, M.; Westphal, A. J.; Wirick, S.; Wooden, D.; Wopenka, B.; Wozniakiewicz, P.; Wright, I.; Yabuta, H.; Yano, H.; Young, E. D.; Zare, R. N.; Zega, T.; Ziegler, K.; Zimmerman, L.; Zinner, E.; Zolensky, M. Comet 81P/Wild 2 Under a Microscope. *Science* **2006**, *314*, 1711–1716.
- (39) Tomeoka, K.; Tomioka, N.; Ohnishi, I. Silicate minerals and Si-O glass in comet Wild 2 samples: Transmission electron microscopy. *Meteorit. Planet. Sci.* **2008**, *43*, 273–284.
- (40) Zolensky, M. E.; Zega, T. J.; Yano, H.; Wirick, S.; Westphal, A. J.; Weisberg, M. K.; Weber, I.; Warren, J. L.; Velbel, M. A.; Tsuchiyama, A.; Tsou, P.; Toppani, A.; Tomioka, N.; Tomeoka, K.; Teslich, N.; Taheri, M.; Susini, J.; Stroud, R.; Stephan, T.; Stadermann, F. J.; Snead, C. J.; Simon, S. B.; Simionovici, A.; See, T. H.; Robert, F.; Rietmeijer, F. J. M.; Rao, W.; Perronnet, M. C.; Papanastassiou, D. A.; Okudaira, K.; Ohsumi, K.; Ohnishi, I.; Nakamura-Messenger, K.; Nakamura, T.; Mostefaoui, S.; Mikouchi, T.; Meibom, A.; Matrajt, G.; Marcus, M. A.; Leroux, H.; Lemelle, L.; Le, L.; Lanzirrotti, A.; Langenhorst, F.; Krot, A. N.; Keller, L. P.; Kearsley, A. T.; Joswiak, D.; Jacob, D.; Ishii, H.; Harvey, R.; Hagiya, K.; Grossman, L.; Grossman, J. N.; Graham, G. A.; Gounelle, M.; Gillet, P.; Genge, M. J.; Flynn, G.; Ferroir, T.; Fallon, S.; Ebel, D. S.; Dai, Z. R.; Cordier, P.; Clark, B.; Chi, M.; Butterworth, A. L.; Brownlee, D. E.; Bridges, J. C.; Brennan, S.; Brearley, A.; Bradley, J. P.; Bleuett, P.; Bland, P. A.; Bastien, R. Mineralogy and Petrology of Comet 81P/Wild 2 Nucleus Samples. *Science* **2006**, *314*, 1735–1739.
- (41) DiSanti, M.; Mumma, M. Reservoirs for Comets: Compositional Differences Based on Infrared Observations. In *Origin and Early Evolution of Comet Nuclei*; Balsiger, H., Altwegg, K., Huebner, W., Owen, T., Schulz, R., Eds.; Springer: New York, 2008; Vol. 28, pp 127–145.
- (42) Greenberg, J. M. Making a comet nucleus. *Astron. Astrophys.* **1998**, *330*, 375–380.
- (43) Hoefen, T. M.; Clark, R. N.; Bandfield, J. L.; Smith, M. D.; Pearl, J. C.; Christensen, P. R. Discovery of Olivine in the Nili Fossae Region of Mars. *Science* **2003**, *302*, 627–630.
- (44) Messenger, S.; Keller, L. P.; Lauretta, D. S. Supernova Olivine from Cometary Dust. *Science* **2005**, *309*, 737–741.
- (45) Kitts, C.; Rasay, R.; Bica, L.; Mas, I.; Neumann, M.; Young, A.; Minelli, G.; Ricco, A. J.; Stackpole, E.; Agasid, E.; Beasley, C.; Friedericks, C.; Squires, D.; Ehrenfreund, P.; Nicholson, W.; Mancinelli, R.; Santos, O.; Quinn, R.; Bramall, N.; Mattioda, A.; Cook, A.; Chittenden, J.; Bryson, K.; Piccini, M.; Parra, M. Initial On-Orbit Engineering Results from the O/OREOS NanoSatellite 25th Annual AIAA/USU. *Conference on Small Satellites*, 2011.
- (46) Colaprete, A.; Schultz, P.; Heldmann, J.; Wooden, D.; Shirley, M.; Ennico, K.; Hermaly, B.; Marshall, W.; Ricco, A.; Elphic, R. C.; Goldstein, D.; Summy, D.; Bart, G. D.; Asphaug, E.; Korycansky, D.; Landis, D.; Sollitt, L. Detection of water in the LCROSS ejecta plume. *Science* **2010**, *330*, 463–468.
- (47) Jubb, A. M.; Allen, H. C. Vibrational Spectroscopic Characterization of Hematite, Maghemite, and Magnetite Thin Films Produced by Vapor Deposition. *ACS Appl. Mater. Interfaces* **2010**, *2*, 2804–2812.
- (48) Patel, M. R.; Christou, A. A.; Cockell, C. S.; Ringrose, T. J.; Zarnecki, J. C. The UV environment of the Beagle 2 landing site: detailed investigations and detection of atmospheric state. *Icarus* **2004**, *168*, 93–115.
- (49) Rottman, G. The SORCE Mission. *Sol. Phys.* **2005**, *230*, 7–25.
- (50) Sherman, D. M.; Waite, T. D. Electronic spectra of Fe³⁺ oxides and oxide hydroxides in the near IR and near UV. *Am. Mineral.* **1985**, *70*, 1262–1269.
- (51) Chernyshova, I. V.; Ponnuram, S.; Somasundaran, P. On the origin of an unusual dependence of (bio)chemical reactivity of ferric hydroxides on nanoparticle size. *Phys. Chem. Chem. Phys.* **2010**, *12*, 14045–14056.
- (52) Cornell, R. M.; Schwertmann, U. The Iron Oxides: Structure, Properties, Reactions, Occurrences and Uses. In *The Iron Oxides: Structure, Properties, Reactions, Occurrences and Uses*; Wiley-VCH: Weinheim, Germany, 2004.
- (53) Marusak, L. A.; Messier, R.; White, W. B. Optical absorption spectrum of hematite, $\alpha\text{Fe}_2\text{O}_3$ near IR to UV. *J. Phys. Chem. Solids* **1980**, *41*, 981–984.
- (54) Nguyen, D. D.; Jones, N. C.; Hoffmann, S. V.; Spanget-Larsen, J. Synchrotron radiation linear dichroism (SRLD) investigation of the electronic transitions of quinizarin, chrysazin, and anthraquinone. *Spectrochim. Acta, Part A* **2010**, *77*, 279–286.
- (55) Navas Diaz, A. Absorption and emission spectroscopy and photochemistry of 1,10-anthraquinone derivatives: a review. *J. Photochem. Photobiol., A* **1990**, *53*, 141–167.
- (56) Skoog, D. A.; West, D. M.; Holler, F. J.; Crouch, S. R. *Fundamentals of Analytical Chemistry*; Brooks/Cole: Belmont, CA, 2013.
- (57) Mishra, H.; Mali, B. L.; Karolin, J.; Dragan, A. I.; Geddes, C. D. Experimental and theoretical study of the distance dependence of metal-enhanced fluorescence, phosphorescence and delayed fluorescence in a single system. *Phys. Chem. Chem. Phys.* **2013**, *15*, 19538–19544.
- (58) Huber, S.; van de Kruijs, R.; Yakshin, A.; Zoethout, E.; Boller, K.-J.; Bijkerk, F. Subwavelength single layer absorption resonance antireflection coatings. *Opt. Express* **2014**, *22*, 490–497.
- (59) Mech, J.; Szacilowski, K. New Type of Photoactive Materials Based on TiO₂ Modified by Anthraquinone Derivatives/Nowe

Fotoaktywne Materiały W Oparciu O TiO_2 Modyfikowany Pochodnymi Antrachinonu. *Arch. Metall. Mater.* **2013**, *58*, 269–273.

(60) Ossowski, T.; Pipka, P.; Liwo, A.; Jeziorek, D. Electrochemical and UV-spectrophotometric study of oxygen and superoxide anion radical interaction with anthraquinone derivatives and their radical anions. *Electrochim. Acta* **2000**, *45*, 3581–3587.